Rashba Splitting in Lead Halide perovskite Nanoribbons

Eric Beery†, Dong Yu‡
† *Physics Department, Haverford College* ‡ *Physics Department, University of California, Davis*

Metal halide perovskites are semiconductor crystals that exhibit promising photovoltaic properties, such as long carrier diffusion lengths, to which long carrier recombination time contributes significantly. The recombination time can be tuned by selecting for either direct or indirect recombination through band splitting due to the Rashba effect. Here we investigate the temperature and photon energy dependence of the Rashba effect by illuminating microcrystal $MAPbBr_3$ with circularly polarized light. We observe strong helicity-dependent photocurrent, with a bandgap reduction as large as 100 meV at room temperature. The helicity-dependent photocurrent blue shifts to the exciton peak (2.3 eV) at lower temperatures, while the total photocurrent peak remains largely unchanged.

Introduction

Metal halide perovskites are metallic crystals with structures ABX_3, where A is a cation, B is a metallic cation, and X is an anion [1]. Perovskites have garnered significant interest over the last decade due to their rapid increase in photovoltaic power conversion efficiency, simple fabrication methods, and potentially low cost. The photovoltaic efficiency is in large part attributed to the perovskite's excellent optoelectronic properties such as long carrier diffusion length, charge recombination time, and a very strong electric field at boundaries due to the charge of the lead nucleus [2, 3]. In the frame of the charge carriers, this large electric field creates a perpendicular magnetic field which interacts with the spin magnetic moment of charge carriers through spin orbit coupling (SOC). Strong SOC can result in Rashba splitting: a spin-dependent splitting of the electronic bands depicted naively in figure 1. Rashba splitting is of great importance to the usefulness of perovskite crystals, as it provides insight into the structure of the material and provides means of tuning the carrier diffusion length via charge recombination time.

Rashba splitting has been theorized in $MAPbBr_3$ through density functional calculations as early as 2015 [3]. Following this theoretical work, Rashba splitting has been observed in both bulk single crystal perovskites and polycrystaline thin films [4, 5]. We instead investigate Rashba splitting in a *micro* single crystal perovskite, as shone in figure 2. This presents distinct advantages over the bulk single crystal as surface effects are larger relative to bulk effects, and a gate voltage can be applied to control the doping of the sample. Furthermore, this single crystal has no grain boundaries, which makes it desirable relative to the thin film configuration.

We observe the amplitude of the Rashba splitting of the electronic bands using the circular photogalvanic effect (CPGE). Through Rashba splitting, a spin $\frac{1}{2}$ carrier's in-plane spin determines which bands the carrier will occupy. Photoexcitation by a circularly polarized photon will excite the carrier to the conduction band. By conservation of angular momentum, a left hand circularly polarized photon will excite a spin-down carrier in the spin-down valence band and flip its spin sign, resulting in a spin-up carrier occupying the spin-up valence band. Similarly, a right hand circularly polarized photon will excite a spin-up carrier into the spin-down conduction band, as shown in figure 1.

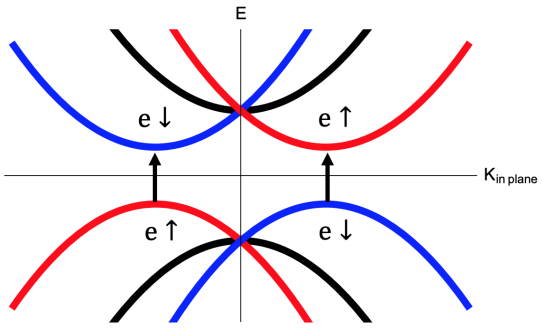

FIG. 1: Band structure plot of Rashba split. The black bands represent the bands without Rashba splitting, the blue band represents the spin down bands, and the red band represents the spin up band.

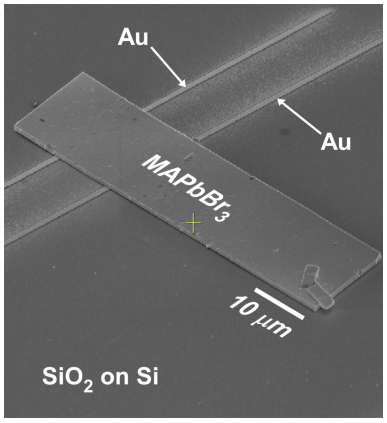

FIG. 2: Single $MAPbBr_3$ nanoribbon laying on top of two gold electrodes.

At high temperatures (230K+), the majority carriers are holes, whereas at lower temperatures the photogenerated carriers form excitons. Therefore, at high temperatures, one would expect a spin up band and a spin down band. Bound carriers in excitons, however, have four possible spin states, and therefore the band splitting may be less intuitive.

In the simple two-band case, the spin up and spin down

bands have opposite momenta. Therefore carriers in these bands will move in opposite directions, yielding a different current dependent on which carriers are excited. If linearly polarized light is shown through a quarter wave plate with fast axis at an angle α to the initial polarization, the light will be left hand circularly polarized for $\alpha = \frac{\pi}{4} + n\pi$ and right hand circularly polarized for $\alpha = \frac{3\pi}{4} + n\pi$. We can then fit the current as a function of α as

$$I = D + L_1 \sin(4\alpha) + L_2 \cos(4\alpha) + C \sin(2\alpha) \quad (1)$$

where D is a DC offset corresponding to photothermal and photovoltaic effects, spin-specified carriers whose spin information has been lost, dark current, etc. L_1 is a direct consequence of the light polarization changing from S (perpendicular to surface) to P (parallel to surface) polarized light, where S polarized light will be absorbed to a greater extent than the P polarized light, as dictated by Fresnel equations. L_2 is a consequence of the linear photogalvanic effect, which we do not discuss here. We are most focused on the C term, which corresponds to the Rashba split, and will be nonzero in the case of a strong Rashba split. A 4α periodicity will result from the first two trigonometric functions, as the light will shift from S and P polarization. A 2α periodicity will arise from the circular photogalvanic effect, as different circular polarization will photoexcite carriers with different momenta.

Methods

We synthesized $MAPbBr_3$ crystals in solution. Lead was deposited onto an fluorine doped tin-oxide glass slide through evaporation deposition using a solution of 60 mg of the precursor $PbAc_2$ in .6 ml of deionized water. This FTO slide was then placed in a solution of 6 mg of $MABr$ to 1 ml of isopropyl alcohol for 72 hours and kept at 40 C. Following this growth period, the FTO slide is removed, dipped in isopropyl alcohol, and gently dried. Crystals from the FTO slides were transferred via an organic microfiber onto a set of gold electrodes on a layer of SiO_2 over a layer of Si.

The crystal and electrode were then placed in a compact optical cryostat (Janis ST-500), with electrical connections established from the crystal to each gold electrode. We performed both AC and DC measurements. For the AC measurement, we applied an AC bias voltage of 0V to 1V at 37Hz from a function generator to the positive electrode, and connected the negative electrode first to a preamp (with a sensitivity of 10^7 V/A) and then to a lock-in amplifier, which was set with a rise-time of 300ms and a sensitivity of 300 mV or 1V depending on the current amplitude. For the DC measurement, a DC bias voltage of 1V was applied,

We then shined a tunable laser through a linear polarizer, a quarter wave plate, and a 10x objective lens onto the crystal at an incident angle of 45 degrees. The quarter wave plate's fast axis makes an angle α with the linear polarization axis. By varying α and recording current, we can fit our currents to equation 1.

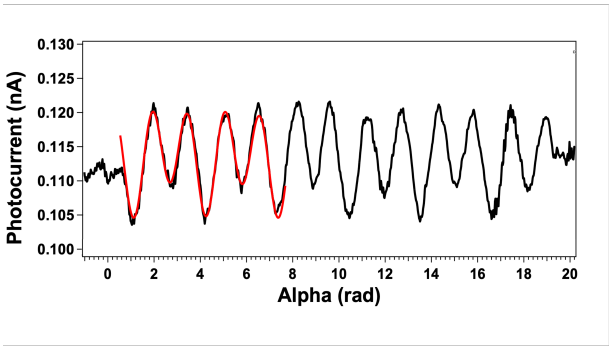

FIG. 3: Plot of photocurrent (nA) versus time, while the QWP rotates through 6π. The function is fit to equation 1 with the following parameters: L1 = .001 nA, L2 = .006 nA, D = .113 nA, C = -.0025 nA.

Results and Discussion

Helicity Dependence of Photocurrent

We recorded the current through the negative electrode over time, and then fit this data to equation 1. A Rashba split is evidenced by a variation in subsequent peak/trough current amplitude. An example of this is shown in figure 3, which was taken with a DC bias at 300 K.

Based on previous CPGE studies [4], we would expect that the amplitude of this C term is dependent on the incident light angle and the orientation of the sample. The sign of the C coefficient has been observed to vary as a function of temperature, as the Rashba split transitions from dynamical at high temperatures to static at low temperatures. Additionally, the C coefficient is expected to significantly diminish at normal light incidence, as symmetry breaking only occurs at the surface and boundaries of the crystal. Finally, by rotating the sample by 180 degrees, the sign of C should change, while the magnitude remains constant, as a 180 degree rotation in effect changes the polarity of photo-injected spins [4].

For data collected at 300K such as that shown in figure 3, the sign of our C term remained negative for all eight DC bias trials under the same incidence angle, sample orientation, and temperature. This can be seen in figure 3 as the first trough, which occurs during left circularly polarized light, is lower than the second trough, which occurs while the light is right circularly polarized. This pattern persists through all DC bias trials, as well as all 300K AC trials as shown in figure 7. There are only two points for 300K in figure 7 due to large noise and erratic data in the other trials.

The sign of the C coefficient is not constant during the lower temperature trials. Under the same sample orientation and incidence angle, the sign of the C term varies between certain wavelengths. For instance, an incident wavelength of 535 nm yielded a current with a C coefficient of .89 nA, which an incident wavelength of 575 nm yielded a current with $c = -.06$ nA, as shown in figure 4. As a consequence of the discrepancy present in the AC bias trials, we did not corroborate the C sign change following a 180 degree sample

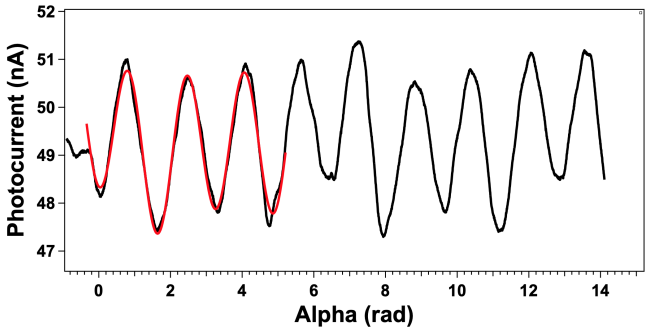

(a) Current measured using an AC bias voltage at 80 K with incident wavelength 535 nm. This current has a positive C coefficient, evidenced by an initial high trough followed by a low trough.

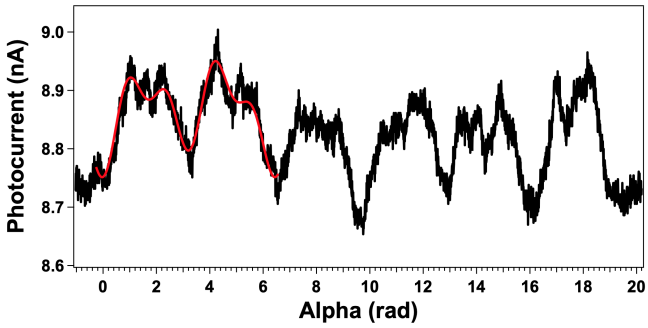

(b) Current measured using an AC bias voltage at 80 K with incident wavelength 575 nm. This current has a negative C coefficient, evidenced by an initial low trough followed by a high trough.

FIG. 4: Two currents recorded that exhibit different C coefficient signs.

rotation.

Bulk single crystal $MAPbBr_3$ has been observed to have two distinct exciton modes at approximately 550 and 555 nm [6]. In micro crystal $MAPbBr_3$, these peaks could occur at different energies. Furthermore, these two modes could exhibit different helicity-dependent responses, which has been observed in polycrystaline thin film perovskites [7], which would explain a difference in the sign of the C term between various frequencies at low temperature.

Photon wavelength dependence

The magnitude of the spin-dependent photocurrent is dependent on the incident photon wavelength. Although this varies on a sample-to-sample basis, the optical band gap of MAPbBr_3 is approximately 2.34 eV at room temperature [8] corresponding to a wavelength of roughly 530 nm. As shown in figure 5, the DC offset, which contributes the majority of the current, peaks at 535 nm. The 300 K data is taken using a

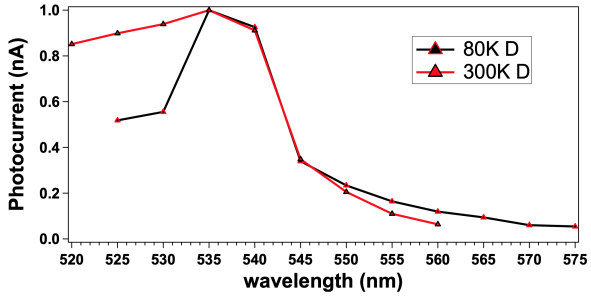

FIG. 5: D coefficient over a range of wavelengths at 80 K and 300 K.

DC bias voltage, whereas the 80 K data was taken using an AC bias, and therefore the two are normalized to 1. It is evident that the higher energy photons (530nm and below) produce less photocurrent at 80 K, which is likely due thermal broadening of the exciton peak at high temperatures, as shown in figure 5.

While the D coefficient relates to the total photoexcitation current, the C term relates only to the spin-dependent photocurrent, which is not so directly related to the optical band gap. As shown in figure 1, the Rashba bands occupy lower energy states than the conduction band, which would indicate that the peak incident wavelength would be longer for C than for D. We observe that the C peak is lower in energy than the D peak at room temperature, and roughly equivalent at 80 K, as shown in figure 6. At 80 K there are C term peaks at the previously mentioned exciton frequencies of 550 nm and 545 nm. The largest peak in the 80K trial is found at 535 nm, which agrees well with the photocurrent spectroscopy peaks found in [8].

The relationship between the C peak and D peak is qualitatively consistent with the findings of [4], who found that the C peak is lower in energy than the PL peak at 290K, and higher than the PL peak at 4K for single crystal $MAPbI_3$.

Despite the C value only showing for four wavelengths at 300 K, we recorded data for the each wavelength shown in figure 5. The reason not all fit coefficients are shown is due to high variability in their values. For plots such as those shown in figure 4a and 4b, the fit parameters vary by very little (roughly 10%) depending on the domain over which the data is fit. For the wavelengths below 545 nm at 300 K, the C coefficient varies by more than 200% depending on where the data is fit. Because of this, the data is excluded from the fit.

Temperature Dependence

Rashba splitting is dependent on the crystalline structure of $MAPbBr_3$, which undergoes temperature-dependent phase transitions from cubic to tetragonal as the temperature drops below roughly 230 K, and from tetragonal to orthorhombic at roughly 140 K. It is therefore informative to investigate the Rashba photocurrent's temperature dependence.

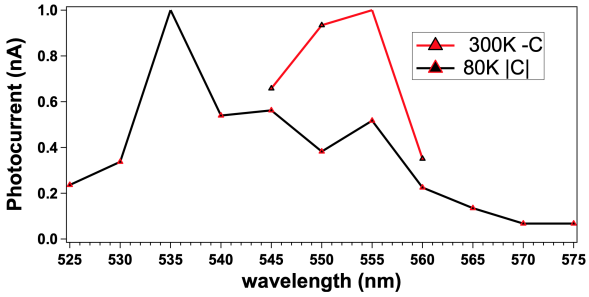

FIG. 6: C coefficient over a range of wavelengths at 80 K and 300 K.

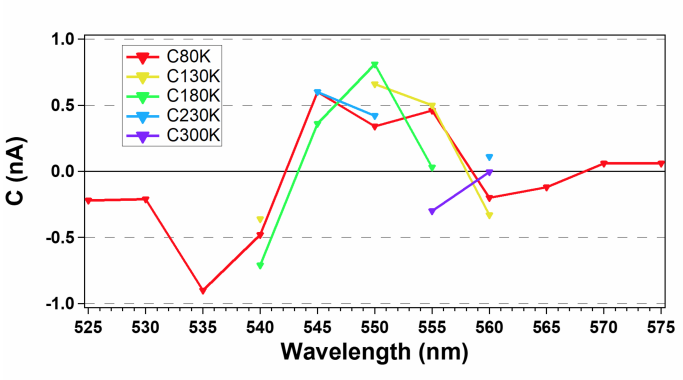

FIG. 7: C term versus incident wavelength at various temperatures as shown in legend.

Figure 7 shows C over various wavelengths at temperatures ranging from 80 K to 300 K. It is clear that a more complete set of data is needed to draw meaningful conclusions. However, this preliminary data presents three qualitative features: 1. The C term has a positive peak at 550 nm, and a negative peak at other energies; 2. The Rashba split is more prevalent at low temperatures; 3. The C term's positive peak redshifts at higher temperatures.

As mentioned in the *Helicity Dependence of Photocurrent* section, different exciton modes with different binding energies have previously been found to exhibit different C term signs [7]. Our data suggests that the Rashba exciton mode with the highest carrier density is at 535 nm, consistent with [8]. We also observe other carrier species with opposite Rashba photocurrent contributions at 535 and 560 nm.

This second qualitative feature is not consistent with the findings of [4]. In their $MAPbI_3$ bulk crystal, they observe that the orthorhombic phase exhibits static Rashba splitting, which is not temperature dependent, whereas the tetragonal phase does exhibit temperature dependence where an increase in temperature increases the amplitude of the Rashba split. Instead, we see that the C magnitude is higher at lower temperatures. Despite this discrepency, $MAPbBr_3$ exhibits an ostensibly static Rashba splitting in the tetragonal and orthorhombic phases, as the C amplitude varies by less than 15%. In the cubic phase, the C amplitude diminishes as the temperature increases.

The third qualitative feature depends on the assumption that the C peak is contained within an incident wavelength of 540 nm to 560 nm. If this assumption is made, then it is apparent that the C peak redshifts at higher temperatures, which is consistent with the findings of [4].

Laser Power

We offer a brief note regarding the incident laser intensity. We've found that an incident intensity of 1 μW for a focused laser (roughly 10 μm spot size) provides a high C amplitude relative to D. For an intensity of 1 μW, the C term is 2.3% as large as the D term, whereas for 3 μW it is 1%, and for .33 μW it is .1%.

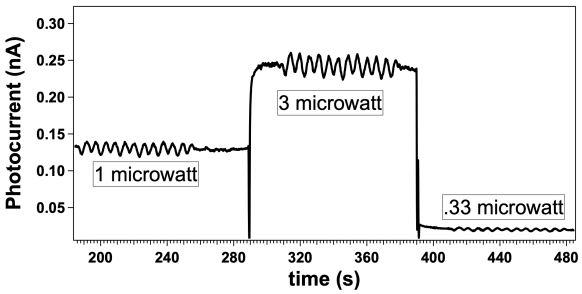

FIG. 8: Photocurrent with varying laser intensity

For a diffuse laser with spot size roughly 50 μm, a higher intensity provides strong Rashba splitting. The data presented in figures 3-7 is taken with an intensity of 4 μW.

Conclusion

We observe helicity-dependent photocurrent in microcrystal $MAPbBr_3$. The bandgap between the valence band and the Rashba conduction band is more than 100 meV smaller than the direct optical bandgap (D) photocurrent peak at 300 K. Towards lower temperatures, the Rashba photocurrent peak blueshifts, until the C peak occurs at the same wavelength as the D peak and the exciton wavelength found by [8]. In the tetragonal and orthorhombic phases, we observe different photexcited carriers with different Rashba splits, where those excited by light with wavelength between 545 nm and 560 nm exhibit positive Rashba photocurrent and those excited by light out of this wavelength range exhibit negative Rashba photocurrent. This indicates that $MAPbBr_3$ has multiple carrier species in these phases with different Rashba interactions. Finally, in the tetragonal and orthorhombic phases, the C peak amplitude varies by less than 15%, which is indicative of a static Rashba effect. At the higher temperature cubic phase, we observe a greater variation in the C amplitude, indicative of a dynamical, temperature dependent Rashba splitting. This

research provides a working foundation for future work into Rashba splitting of microcrystal $MAPbBr_3$.

Acknowledgements

I would like to thank Prof. Dong Yu for excellent mentorship during the UC Davis REU. This work would have been impossible without the help and teaching of Tony Song, Luke McClintok, Clark Travaglini, and Bob Wang. I would like to thank Prof. Rena J. Zieve and Prof. Nicholas Curro for organizing the REU program, funded by NSF grant PHY-1852581.

[1] Y. Jiang, X. Wang, and A. Pan, Advanced Materials **31**, 1806671 (2019), ISSN 1521-4095, _eprint: https://onlinelibrary.wiley.com/doi/pdf/10.1002/adma.201806671, URL https://onlinelibrary.wiley.com/doi/abs/10.1002/adma.201806671.

[2] N.-G. Park, Materials Today **18**, 65 (2015), ISSN 1369-7021, URL https://www.sciencedirect.com/science/article/pii/S1369702114002570.

[3] M. Kepenekian, R. Robles, C. Katan, D. Sapori, L. Pedesseau, and J. Even, ACS Nano **9**, 11557 (2015), ISSN 1936-0851, publisher: American Chemical Society, URL https://doi.org/10.1021/acsnano.5b04409.

[4] D. Niesner, M. Hauck, S. Shrestha, I. Levchuk, G. J. Matt, A. Osvet, M. Batentschuk, C. Brabec, H. B. Weber, and T. Fauster, Proceedings of the National Academy of Sciences **115**, 9509 (2018), ISSN 0027-8424, 1091-6490, URL http://www.pnas.org/lookup/doi/10.1073/pnas.1805422115.

[5] B. Zhou, L. Liang, J. Ma, J. Li, W. Li, Z. Liu, H. Li, R. Chen, and D. Li, Nano Letters **21**, 4584 (2021), ISSN 1530-6984, 1530-6992, URL https://pubs.acs.org/doi/10.1021/acs.nanolett.1c00364.

[6] T. Thu Ha Do, A. Granados del Águila, C. Cui, J. Xing, Z. Ning, and Q. Xiong, Phys. Rev. B **96**, 075308 (2017), URL https://link.aps.org/doi/10.1103/PhysRevB.96.075308.

[7] J. Li and P. M. Haney, Applied Physics Letters **109**, 193903 (2016), ISSN 0003-6951, 1077-3118, URL http://aip.scitation.org/doi/10.1063/1.4967176.

[8] L. McClintock, Z. Song, H. C. Travaglini, R. T. Senger, V. Chandrasekaran, H. Htoon, D. Yarotski, and D. Yu (Submitted 2021).